Indian Journal of Chemistry
Vol. 63, May 2024, pp. 457-463
DOI: 10.56042/ijc.v63i5.8279

Synthesis and magnetic properties of perovskite manganite $La_{0.8}Ca_{0.15}Na_{0.05}Mn_{0.8}Fe_{0.2}O_3$

Suram Singh[a], Mukesh Kumar Verma[b] & Devinder Singh*[c]

[a] Higher Education Department, Govt. of Jammu and Kashmir, Jammu 180 004, India

[b] Department of Chemistry, Swami Shraddhanand College, University of Delhi, Delhi 110 036, India

[c] Department of Chemistry, University of Jammu, Jammu 180 006, India

E-mail: suram_cheerful@rediffmail.com, mkvermachem@gmail.com, drdssambyal@rediffmail.com

Received 24 January 2024; accepted (revised) 23 April 2024

The current study describes the synthesis of the perovskite manganite $La_{0.8}Ca_{0.15}Na_{0.05}Mn_{0.8}Fe_{0.2}O_3$ using Pechini method. The Rietveld analysis of the powder X-ray diffraction data verified the presence of a single phase exhibiting orthorhombic symmetry with the *Pnma* space group. The phase undergoes a shift from paramagnetism to ferromagnetism when the temperature reaches the Curie temperature of 111 K. A positive Weiss constant (Θ) and a greater effective magnetic moment than the anticipated value suggests the presence of dominating ferromagnetic interactions in the phase.

Keywords: Pechini method, Rietveld refinements, Magnetic properties

The standard formula for mixed-valence perovskite manganites is $RE_{1-y}A_yMn_{1-x}B_xO_3$, where RE represents a trivalent in nature rare earth ion, A represents a divalent in nature alkaline earth metals like Ca, Sr, Ba, or a monovalent alkali metal such as Na or K, and B represents ions made of transition metals or nonmagnetic trivalent ions such as Al, Ga, or In. The substituted manganites continue to captivate researchers in the field of solid-state chemistry, as evidenced by the extensive study conducted thus far[1–7]. Materials with high susceptibility to outside factors including magnetic field, pressure, temperature, and electricity have demonstrated significant promise in several applications including magnetic storage, magnetic sensors, magnetic refrigeration, spin-valve devices, and optical instruments[8–13]. These materials experience a change from a state of being paramagnetic and semiconducting to a state of being ferromagnetic and metallic as the temperature decreases. This change is indicated by a peak in resistivity at a temperature called T_{MS}, which is in close proximity to the transition temperature from paramagnetic (PM) to ferromagnetic (FM) states, known as the Curie temperature T_C. Furthermore, these materials demonstrate a significant magneto-resistance effect, characterised by a reduction in electrical resistivity when subjected to a magnetic field[14–17]. The Zener double exchange (DE) interaction, which involves the coupling of spin and orbital structure[18], as well as the Jahn-Teller (JT) distortions[19], can be linked to the transition from a paramagnetic-semiconductor to a ferromagnetic metal at low temperatures. Furthermore, the primary factors that influence the distinct properties of manganites are the average size of cations at the A-site ($<r_A>$)[20], the disorder caused by the mismatch in cation sizes at the A-site (σ^2)[21], the technique of manufacture, the magnetic field, and the level of oxygen deprivation. The doping of such materials can modify their physical properties, which are predominantly influenced by factors such as concentration, ionic size, and the oxidation state of the dopant[22].

Extensive research has been conducted on the doping of A-site with divalent or monovalent ions in order to get a more profound comprehension of the structural and magnetic characteristics of doped perovskites[3,4,6,7,23–25]. An intriguing area of study is investigating the impact of Mn–site doping in manganites, which has a significant impact on the structural and magnetic characteristics. This is achieved by altering the carrier density (n), Mn–O–Mn bond angle, and Mn–O bond length. Doping of Mn in perovskite manganites with trivalent ions like Al^{3+}, Bi^{3+}, Ru^{3+}, and Co^{3+} decreases the ratio of Mn^{3+} to Mn^{4+} and suppresses Curie temperature

T_C[26–31]. Multiple researchers have examined the impact of substituting a portion of manganese (Mn) with iron (Fe) on the structural and magnetic characteristics[32–50]. These manganites possess a composite structure consisting of Mn^{3+} and Fe^{3+} ions at octahedral (B) sites. The replacement of Mn ions with Fe ions in manganites not only causes distortions in the lattice structure but additionally decreases the Mn^{3+}/Mn^{4+} ratio, resulting in the suppression of Curie temperature T_C. The $La_{0.67}Ca_{0.33}Mn_{1-x}Fe_xO_3$ perovskite system (with x values of 0.00, 0.01, 0.03, and 0.07) exhibits a transformation from PM to FM behaviour when the temperature lowers. As the temperature drops, the perovskite $La_{0.67}Ca_{0.33}Mn_{1-x}Fe_xO_3$ (with x values of 0.00, 0.01, 0.03 and 0.07) exhibits ferromagnetic (FM) behaviour instead of paramagnetic (PM) behaviour. The transition temperature from PM to FM decreases as the content of Fe increases[41]. The magnetization experiments of $La_{0.6}Ca_{0.4}Mn_{1-x}Fe_xO_3$ (with x values of 0, 0.05, 0.1, 0.15 and 0.2) revealed that the introduction of Fe atoms results in lowering of T_C from 275 K (x = 0) to 75 K (x = 0.2). Additionally, for a critical composition of $x \geq 0.1$, there is a simultaneous presence of ferromagnetic and antiferromagnetic interactions[43]. In their study, Sahasrabudhe *et al*.[45] found that in the examined system $La_{0.7}Ca_{0.3}Mn_{1-x}Fe_xO_3$ (with x values of 0.08, 0.1 and 0.12), there is only one ferromagnetic phase present below the transition temperature, and no spin glass behaviour was seen. Kundaliya *et al*.[48] have previously reported similar findings for the combination $La_{0.67}Ca_{0.33}Mn_{0.9}Fe_{0.1}O_3$. The decrease in both ferromagnetism and conduction in the ferromagnetic (x = 0.37) and antiferromagnetic (x = 0.53) phases of $La_{1-x}Ca_xMnO_3$ when Fe-doped, is caused by the lowering of DE interactions and the depopulation of hopping electrons[49]. The substitution of Mn^{3+} with Fe^{3+} in the $La_{0.67}Ca_{0.33}Mn_{0.9}Fe_{0.1}O_3$ perovskite material decreases the number of available hopping sites for the Mn e_g (up) electrons, leading to a decrease in ferromagnetic exchange. At low temperatures, the system enters a randomly canted ferromagnetic state due to competition amongst co-existing antiferromagnetic super-exchange interactions and the ferromagnetic DE interactions[50].

We have previously documented the structural and magnetic characteristics of iron-doped perovskite manganites $La_{0.8}Ca_{0.15}Na_{0.05}Mn_{1-x}Fe_xO_3$ (with x values of 0, 0.05, 0.10 and 0.15) that were synthesized using Pechini method[51]. The results indicated a negative correlation between the concentration of the dopant (Fe) and the T_C, with the T_C falling as the concentration of the dopant increased. Our analysis was restricted to examining the dopant concentration up to a maximum value of x = 0.15. In order to examine the effects of substituting a greater doping level of Fe at the B-site on the structural and magnetic characteristics, we have synthesized Fe-doped $La_{0.8}Ca_{0.15}Na_{0.05}Mn_{0.8}Fe_{0.2}O_3$ manganite using a modified sol-gel Pechini process and investigated its magnetic and structural characteristics.

Experimental Section

The polycrystalline sample with composition $La_{0.8}Ca_{0.15}Na_{0.05}Mn_{0.8}Fe_{0.2}O_3$ has been synthesized by the Pechini method using ultra-pure (99.9%) La_2O_3, $CaCO_3$, Na_2CO_3, $Mn(CH_3COO)_2.4H_2O$, and $Fe(NO_3)_3.9H_2O$ as starting materials. The lanthanum oxide underwent a firing process at a temperature of 1000°C for 6h to eliminate any moisture and adsorbed gases before being weighed. At first, the reactants were dissolved in 3N nitric acid and stirred continuously at 80°C for two hours to guarantee the generation of metal nitrates. The metal nitrates underwent conversion to citrates with the addition of a suitable quantity of citric acid (3 moles for every 1 mole of metal ion). The pH of the citrate solution was modulated to a range of 6.5 to 7 by incrementally adding drops of ammonia solution. Next, the solution was supplemented with the necessary quantity of ethylene glycol (4 moles for every 1 mole of metal ion), which acts as a polymerization agent. The solution was then agitated for approximately 2h to promote the polymerization process. Subsequently, the solution was gradually evaporated at 90°C on a thermal plate to ensure complete elimination of the solvent, leading to the production of a uniform and thick gel. The gel was dehydrated at a temperature of 250°C using a hot air oven to obtain a dry, porous substance. This substance was then subjected to a temperature of 500°C for 8h in a muffle furnace. The resulting product was pulverized into a fine powder and subsequently compacted into a pellet employing a hydraulic press under pressure of about 20 MPa. The pellet underwent calcination at a temperature of 1000°C for 10h to achieve the desired composition. In the electric tube furnace, the sample was lastly progressively cooled to ambient temperature.

The powder sample was structurally characterized using powder X-ray diffraction (XRD). Utilising a

computerised powder X-ray diffractometer (PANalytical X′PERT-PRO MPD) from the Netherlands, the XRD analyses were conducted at ambient temperature. The device ran at 45 kV and 40 mA and was outfitted with Ni-filtered CuKα radiation (λ = 1.54443 Å). The XRD research was performed in the 10° to 100° 2θ range. The topography and microstructure of the powdered sample were analyzed using Scanning Electron Microscopy (SEM) with an accelerating voltage ranging from 0.3 to 30 kV. Energy-dispersive X-ray spectroscopy (EDX) employing an INCA attachment to a SEM device was used to investigate the compositional purity and stoichiometry of different cations.

The powder sample was subjected to temperature-dependent magnetization (χ_m–T) measurements under zero-field cooled (ZFC) and field-cooled (FC) conditions. These measurements were conducted using a Faraday magnetic balance equipped with a Polytronic electromagnet. The magnetic investigation was conducted within the temperature range of liquid nitrogen, using an applied magnetic field of 1000 G.

Results and Discussion

Structural characterization

The crystal structure and the phase purity of the $La_{0.8}Ca_{0.15}Na_{0.05}Mn_{0.8}Fe_{0.2}O_3$ sample were examined employing powder XRD at ambient temperature. Fig. 1(a) depicts the XRD spectrum of the synthesized compound. The sample exhibited distinct and prominent peaks that closely resembled the perovskite structure, suggesting a high degree of crystallinity. No secondary phase was observed within the instrument's sensitivity limit. All the recorded diffraction maxima were indexed perfectly in the orthorhombic setting of the *Pnma* space group. We used the GSAS/EXPGUI programme to perform Rietveld refinement on the XRD data in order to get detailed information on the prepared sample's crystal structure[52]. This involved incorporating a substantial amount of structural information from the literature, specifically in the space group *Pnma*. In this space group, the La/Ca/Na atoms were found to be located at the 4c(x, 0.25, z) position, while the Mn/Fe atoms were located at the 4b(0, 0, 0.5) position. Additionally, the oxygen atoms were found to occupy two different sites: O1 at the 4c(x, 0.25, z) position and O2 at the 8d(x, y, z) position. The occupancy factors for the metals were determined by taking the sample stoichiometry into account, whereas the occupation factors for oxygen atoms were refined. The XRD structural refinement did not provide any indication of oxygen non-stoichiometry. As a result, the oxide ion sites were assumed to be fully occupied. The Rietveld profile fitting for the data is shown in Fig. 1(b). The presence of a phase with great purity has been confirmed by the strong correlation between the calculated and observed diffraction patterns. Table 1 presents the precise structural parameters, dependable parameters R_p, R_{wp} and reduced χ^2 value acquired using the Rietveld analysis. The values of obtained reliable parameters R_{wp}, R_p and χ^2 confirmed the crystal structure of the synthesized perovskite manganite using Rietveld analysis.

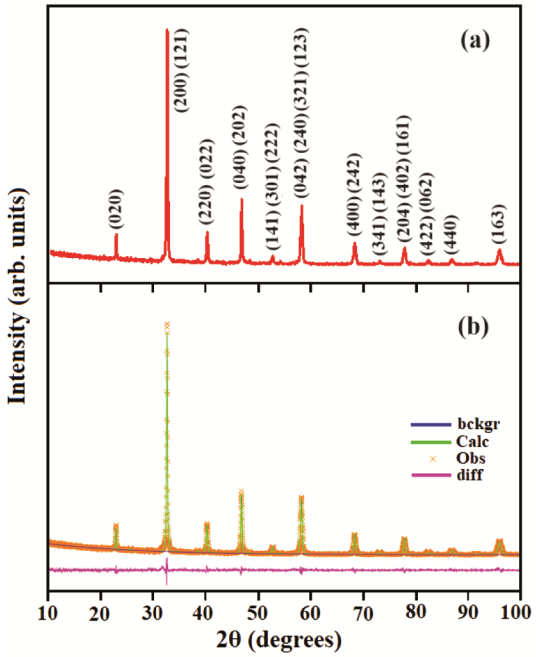

Fig. 1 — (a) Typical Miller-indexed XRD pattern and (b) Rietveld profile fitting for the XRD pattern of $La_{0.8}Ca_{0.15}Na_{0.05}Mn_{0.8}Fe_{0.2}O_3$

Table 1 — Structural Parameters of $La_{0.8}Ca_{0.15}Na_{0.05}Mn_{0.8}Fe_{0.2}O_3$ phase

Atom	site	x	y	z	U_{iso} (Å^2)
La/Ca/Na	4c	0.0156(3)	0.25	–0.0024(3)	0.02042(5)
Mn/Fe	4b	0	0	0.5	0.01412(6)
O(1)	4c	0.4968(22)	0.25	0.0698(22)	0.06007(6)
O(2)	8d	0.2665(14)	0.0285(14)	–0.2725(14)	0.02701(5)

Space group *Pnma*, a = 5.4772(3) Å, b = 7.7514(5) Å, c = 5.5049(3) Å, V = 233.72(2) Å^3, R_{wp} = 0.1223, R_p = 0.0894, χ^2 = 1.03

The selected Mn/Fe–O–Mn/Fe bond angles and Mn/Fe–O bond lengths, along with their averages, are presented in Table 2. Examination of bond lengths and bond angles reveals substantial distortion in the $(Mn/Fe)O_6$ octahedra. The angles Mn/Fe–O(1)–Mn/Fe and Mn/Fe–O(2)–Mn/Fe in the ideal cubic perovskite structure, are expected to be 180°. However, in our sample under investigation, these angles deviate from this value due to the tilting of the octahedra.

The mean size of the crystallites (D) was computed based on the XRD patterns using the Scherrer formula as stated in reference[53]

$$D = \frac{K\lambda}{\beta \cos\theta}$$

The shape factor, denoted as K, is equal to 0.90, λ represents the wavelength of the X-ray, θ defines the position of the peak, and β represents the full width at half maximum of the peak, measured in radians. The determined value of the mean crystallite size (D) was 41.1 nm. The compound's nanometric size is attributed to the modest synthesis temperature, usually about 1000°C, achieved by the sol-gel technique.

Elemental and microstructural analysis

The synthesized sample was subjected to EDX analysis to evaluate the stoichiometry and compositional purity of its constituent elements. The EDX spectrum of the $La_{0.8}Ca_{0.15}Na_{0.05}Mn_{0.8}Fe_{0.2}O_3$ sample, displayed in Fig. 2, validates the existence of all constituent elements within the compound. The mass proportion of different regions has been used to calculate a typical cationic composition. The results (expressed as mass percentages) confirm that there is minimal loss of constitutive elements during the preparation process, and no presence of impurity was detected within the experimental constraints. Due to its lower atomic weight, O cannot be accurately detected by EDX. Therefore, only the chemical composition of La, Ca, Na, Mn, and Fe is shown in Table 3. The agreement between the experimental and theoretical mass percentages indicates that the cation composition in the sample has been confirmed.

The SEM technique was used to examine the topography and microstructure of the prepared phase. Fig. 3 displays the SEM image of the $La_{0.8}Ca_{0.15}Na_{0.05}Mn_{0.8}Fe_{0.2}O_3$ powder, providing a realistic visual representation of its structure under a scanning electron microscope. The SEM analysis reveals a polycrystalline structure in the as-synthesized sample, characterized by a random distribution of grains with varying shapes. There is a certain amount of agglomeration among the grains,

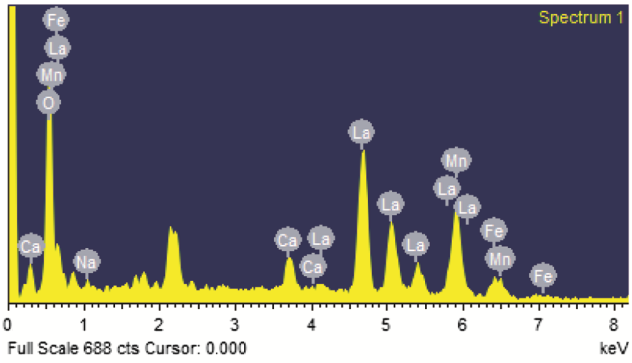

Fig. 2 — EDX spectrum of $La_{0.8}Ca_{0.15}Na_{0.05}Mn_{0.8}Fe_{0.2}O_3$

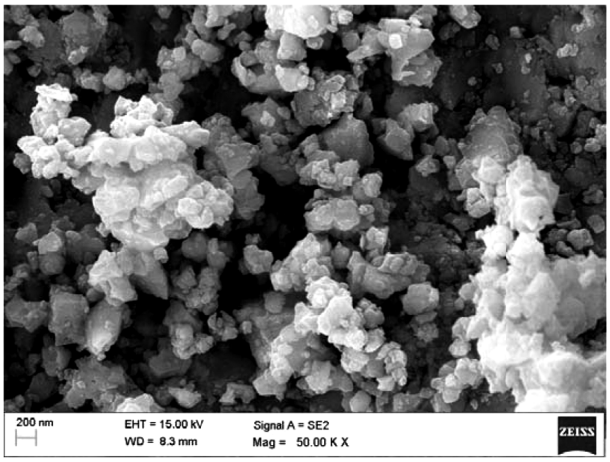

Fig. 3 — SEM micrograph of polycrystalline powder of $La_{0.8}Ca_{0.15}Na_{0.05}Mn_{0.8}Fe_{0.2}O_3$

Table 2 — Selected bond lengths (Å) and bond angles (º) and their averages for $La_{0.8}Ca_{0.15}Na_{0.05}Mn_{0.8}Fe_{0.2}O_3$

Mn/Fe – O(1)×2	1.97560(12)
Mn/Fe – O(2)×2	1.93590(7)
Mn/Fe – O(2)×2	1.98366(7)
<Mn/Fe – O>	1.96505
Mn/Fe – O(1) – Mn/Fe	157.558(2)
Mn/Fe – O(2) – Mn/Fe	164.290(1)
<Mn/Fe – O – Mn/Fe>	160.924

Table 3 — EDX results of $La_{0.8}Ca_{0.15}Na_{0.05}Mn_{0.8}Fe_{0.2}O_3$

Element	Mass (%)	
	Observed	Calculated
La	49.85	50.19
Ca	2.66	2.71
Na	0.46	0.52
Mn	19.65	19.85
Fe	4.95	5.04

with diameters in the nanometric range. The existence of certain pores in the sample is likely associated with the preparation method of citrate precursors.

Magnetic Properties

Fig. 4 displays the molar magnetic susceptibility *versus* temperature ($\chi_m - T$) curve for the $La_{0.8}Ca_{0.15}Na_{0.05}Mn_{0.8}Fe_{0.2}O_3$ sample. The measurements were taken under both ZFC and FC modes. Our synthesized sample has shown a rise in susceptibility as the temperature is lowered. This is characterized by a shift from a typical PM to FM phase at low temperatures, which is known as T_C. The ferromagnetic behaviour in divalent/monovalent ion-doped perovskite manganite is attributed to the presence of Mn in a mixed-valence state of +3 and +4, which leads to the formation of Mn^{3+}/Mn^{4+} pairs. The presence of Mn^{3+}/Mn^{4+} pairs results in a double exchange (DE) interaction, which involves the magnetic coupling between these pairs. This mechanism is attributed to the ferromagnetism seen in this manganite[6,7,54]. The T_C value is obtained by identifying the minima on the $d\chi_m/dT$ *vs* T curve, which is shown as an inset in Fig. 4. The calculated T_C value is 111 K. The value of Curie temperature obtained is consistent with the results reported earlier[51,55].

As expected, the substitution of the Mn site by a higher doping level of Fe does not vanish the ferromagnetic state noticed at a lower temperature in the parental sample $La_{0.8}Ca_{0.15}Na_{0.05}MnO_3$ but

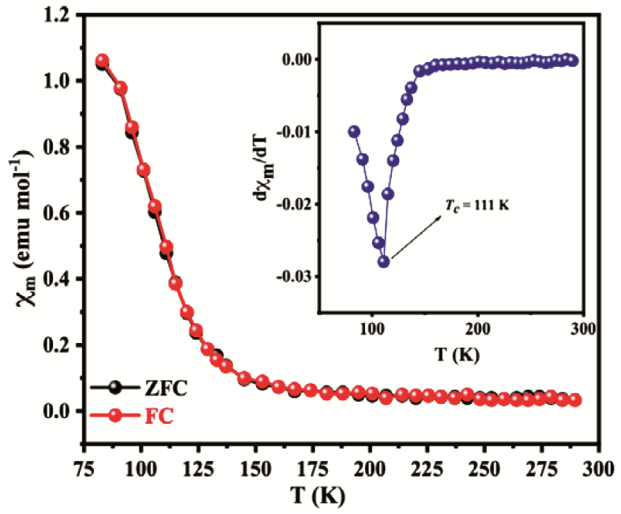

Fig. 4 — Temperature dependence of molar magnetic susceptibility for $La_{0.8}Ca_{0.15}Na_{0.05}Mn_{0.8}Fe_{0.2}O_3$. (Inset shows the variation of $d\chi_m/dT$ as a function of temperature (T) for $La_{0.8}Ca_{0.15}Na_{0.05}Mn_{0.8}Fe_{0.2}O_3$)

decreases the T_C remarkably which can be credited to the competition among the double exchange (Mn^{3+}–O–Mn^{4+}) and the super-exchange interactions (Mn^{3+}–O–Mn^{3+} and Mn^{4+}–O–Mn^{4+})[56]. The Mn^{3+}/Mn^{4+} ratio is lowered when Fe is doped because Fe^{3+} replaces Mn^{3+}. Furthermore, there is no participation of the Fe^{3+} ions in the DE interaction with the Mn^{4+} ions. Consequently, the ferromagnetic DE interaction is attenuated in favour of super-exchange interactions, leading to a reduction in T_C.

Fig. 5 displays the temperature dependence of the reciprocal ZFC molar magnetic susceptibility for the given phase. The $\chi_m^{-1} - T$ curve's linearity suggests that the Curie-Weiss law, which is established by the following relationship:

$$\chi_m = \frac{C}{T - \Theta}$$

where C is the Curie constant and Θ is the Curie-Weiss temperature, is followed in the high-temperature region, where the sample is completely paramagnetic. The value of Curie-Weiss temperature (Θ) has been considered as that temperature at which the straight line fit of χ_m^{-1} *versus* T plot of paramagnetic region meets the X-axis. The value of Θ is calculated from the plot by extrapolation of the straight line fit of the curve towards the temperature axis, whereas the slope of the curve defines the value of the Curie constant (C). The values of Θ and C are determined to be 59 K and 6.663 respectively. The positive value of Θ suggests that ferromagnetic interactions are the prevailing factor in the phase. Furthermore, the observed decrease in the Θ value in

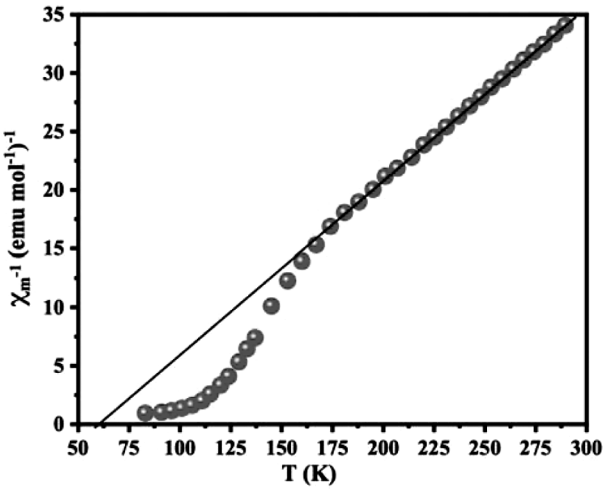

Fig. 5 — Plot of temperature-dependent inverse molar magnetic susceptibility for the $La_{0.8}Ca_{0.15}Na_{0.05}Mn_{0.8}Fe_{0.2}O_3$

comparison to our previously reported system[51], provides additional evidence of the gradual reduction in long-range ferromagnetic exchange interaction due to disorder.

The effective magnetic moment (μ_{eff}) of the phase within the temperature range where the Curie-Weiss rule is applicable has been calculated using the Curie constant (C) according to the following equation:

$$\mu_{eff} = 2.828\sqrt{C}$$

The theoretical magnetic moment value (μ_{cal}) of the $La_{0.8}Ca_{0.15}Na_{0.05}(Mn^{3+}_{0.55}Mn^{4+}_{0.25})Fe_{0.2}O_3$ phase has been calculated from the relationship[6,7,54]

$$\mu_{cal} = \sqrt{0.55\mu^2_{Mn^{3+}} + 0.25\mu^2_{Mn^{4+}} + 0.2\mu^2_{Fe^{3+}}}$$

where $\mu_{Mn^{3+}}$, $\mu_{Mn^{4+}}$ and $\mu_{Fe^{3+}}$ are the spin-only magnetic moments of Mn^{3+} (4.90 B.M.), Mn^{4+} (3.87 B.M.) and Fe^{3+} (5.92 B.M.) ions in their high spin states respectively. The values of μ_{eff} and μ_{cal} were determined to be 7.30 B.M. and 4.89 B.M. respectively. The higher value of μ_{eff} compared to μ_{cal}can be credited to the existence of ferromagnetic interactions within the magnetic structure of this polycrystalline phase.

Conclusions

The perovskite manganite $La_{0.8}Ca_{0.15}Na_{0.05}Mn_{0.8}Fe_{0.2}O_3$, prepared by sol-gel based Pechini method, crystallized in the orthorhombic symmetry with *Pnma* space group. The phase exhibits dominant ferromagnetic interactions attributed to the presence of Mn in a mixed-valence state of +3 and +4 leading to the formation of Mn^{3+}/Mn^{4+} pairs which are accountable for the creation of ferromagnetic double exchange interactions. The value of the effective magnetic moment was found to be higher than that of the calculated one indicating that ferromagnetic interactions are prevalent in the phase. The dominant ferromagnetic behaviour of the phase was further confirmed by the positive value of the Weiss constant (Θ).

References

1 Xia W, Li L, Wu H, Xue P & Zhu X, *Ceram Int*, 43 (2017) 3274.
2 Sfirloaga P, Poienar M, Malaescu I, Lungu A, Mihali C V & Vlazan P, *Ceram Int*, 44 (2018) 5823.
3 Li Y, Zhang H, Chen Q, Li D, Li Z & Zhang Y, *Ceram Int*, 44 (2018) 5378.
4 Sun T, Zhao S, Ji F & Liu X, *Ceram Int*, 44 (2018) 2400.
5 Li S B, Wang C B, Zhou D Q, Liu H X, Li L, Shen Q & Zhang L M, *Ceram Int*, 44 (2018) 550.
6 Verma M K, Sharma N D, Sharma S, Choudhary N & Singh D, *J Alloys Compd*, 814,(2020) 152279.
7 Verma M K, Sharma N D, Sharma S, Choudhary N & Singh D, *Mater Res Bull*, 125,(2020) 110813.
8 Bridges F, Booth C H, Kwei G H, Neumeir J J & Swatzky G A, *Phys Rev B*, 61 (2000) 9237.
9 Awana V P S, Tripathi R, Kumar N, Kishan H, Bhalla G L, Zeng R, Chandra L S S, Ganesan V & Habermeier H U, *J Appl Phys*, 107 (2010) 09D723.
10 Haghiri-Gosnet A M & Renard J P, *J Phys D:Appl Phys*, 36 (2003) R127.
11 Samanta T, Das I & Banerjee S, *Appl Phys Lett*, 91 (2007) 082511.
12 Moreo A, Yunoki S & Dagotto E, *Science*, 283 (1999) 2034.
13 Mahato R N, Sethupathi K, Sankaranarayanan V & Nirmala R, *J Magn Magn Mater*, 322 (2010) 2537.
14 Maji C, *Curr Sci*, 112 (2017) 1390.
15 Skini R, Khlifi M, Wali M, Dhahri E & Hlil E K, *J Magn Magn Mater*, 363 (2014) 217.
16 Zaidi N, Mnefgui S, Dhahri A, Dhahri J & Hlil E K, *J Alloys Compd*, 616 (2014) 378.
17 Zaidi A, Alharbi T, Dhahri J, Alzobaidi S, Zaidi M A & Hlil E K, *Appl Phys A*, 123 (2017) 94.
18 Ishihara S, Inoue J & Maekawa S, *Phys Rev B*, 55 (1997) 8280.
19 Millis A J, Littlewood P B & Shraiman B I, *Phys Rev Lett*, 74 (1995) 5144.
20 Hwang H Y, Cheong S W, Radaelli P G, Marezio M & Batlogg B, *Phys Rev Lett*, 75 (1995) 914.
21 Rodriguez-Martinez L M & Attfield J P, *Phys Rev B*, 54 (1996) R15622.
22 Mazur A, Steevendaal U V, Buse K, Weber M, Schirmer O F, Hesse H & Krätzig E, *Appl Phys B*, 65 (1997) 481.
23 Khlifi M, Bejar M, El Sadek O, Dhahri E, Ahmed A M & Hlil E H, *J Alloys Comp*, 509 (2011) 7410.
24 Muroi M, Street R & McComik P G, *J Appl Phys*, 87 (2000) 3424.
25 Szewczyk A, Gutowska M, Dabrowski B, Plackowski T, Danilova N P & Gaidukov Y P, *Phys Rev B*, 71 (2005) 224432.
26 Dhahri J, Dhahri A, Oumezzine M & Dhahri E, *J Magn Magn Mater*, 320 (2008) 2613.
27 Dhahri N, Dhahri A, Cherif K, Dhahri J, Taibi K & Dhahri E, *J Alloys Comp*, 496 (2010) 69.
28 Zarifi M, Kameli P, Nouraddini M I, Kotsedi L & Maaza M, *J Alloys Comp*, 792 (2019) 1095.
29 Jethva S, Katba S, Udeshi M & Kuberkar D G, *Physica B: Condensed Matter*, 520 (2017) 13.
30 Rathod J S, Khachar U, Doshi R R, Solanki P S & Kuberkar D G, *Int J Mod Phys B*, 26 (2012) 1250136.
31 Krichene A, Solanki P S, Rayaprol S, Ganesan V, Boujelben W & Kuberkar D G, *Ceram Int*, 41 (2015) 2637.
32 Nasri A, Zouari S, Ellouze M, Rehspringer J L, Lehlooh A F & Elhalouani F, *J Supercond Novel Magn* 27 (2014) 443.
33 Zouari S, Ellouze M, Hlil E K, Elhalouani F & Sajieddine M, *Solid State Commun*,180 (2014) 16.
34 Zouari S, Nasri A, Ellouze M, Hlil E K & Elhalouani F, *J Supercond Novel Magn*, 6 (2013) 2435.

35 Apandi N A, Ibrahim N, Awang Z, Azis R S, Syazwan M M & Yahya A K, *Materials Science and Engineering: B*, 276 (2022) 115562.

36 Al-Shahumi T M, Al-Omari I A, Al-Harthi S H, Myint M T, Kharel P, Lamichhane S & Liou S H, *J Alloys Comp*, 958 (2023) 170454.

37 Zouari S, Ellouze M, Hlil E K, Elhalouani F & Sajieddine M, *Solid State Commun*, 180 (2014) 16.

38 Ghosh K, Ogale S B, Ramesh R, Greene R L, Venkatesan T, Gapchup K M, Bathe R & Patil S I, *Phy Rev B,* 59 (1999) 533.

39 Rao G H, Sun J R, Kattwinkel A, Haupt L, Bärner K, Schmitt E & Gmelin E, *Physica B*, 269 (1999) 379.

40 Huo G, Song D, Yang Q & Dong F, *Ceram Int*, 34 (2008) 497.

41 Liu X J, Li Z Q, Wu P, Bai H L & Jiang E Y, *Solid State Commun*, 142 (2007) 525.

42 Dayal V & Keshri S, *Solid State Commun*, 142 (2007) 63.

43 Othmani S, Balli M & Cheikhrouhou A, *Solid State Commun*, 192 (2014) 51.

44 Simopoulos A, Pissas M, Kallias G, Devlin E, Moutis N, Panagiotopoulos I, Niarchos D , Christides C & Sonntag R, *Phys Rev B,* 59 (1999) 1263.

45 Sahasrabudhe M S, Patil S I, Date S K, Adhi K P, Kulkarni S D, Joy P A & Bathe R N, *Solid State Commun*, 137 (2006) 595.

46 Granja L, Indelicato E, Levy P, Polla G, Vega D & Parisi F, *Physica B*, 320 (2002) 94.

47 Zhang G & Lin J, *J Alloys Compd,* 507 (2010) 47.

48 Kudaliya D C, Vij R, Kulkarni R G, Tulapurkar A A, Pinto R, Malik S K & Yelon W B, *J Magn Magn Mater*, 264 (2003) 62.

49 Ahn K H, Wu X W, Liu K & Chien C L, *J Appl Phys*, 81 (1997) 5505.

50 Yusuf S M, Sahana M, Hedge M S, Dörr K & Müller K H, *Phys Rev B*, 62 (2000) 1118.

51 Singh S & Singh D, *J Alloys Compd*, 702, 249 (2017)

52 Larson A C &. Von Dreele R B, *Generalized structure analysis system (GSAS), Los Alamos National Laboratory*, (1994) 86.

53 Klug H P & Alexander L E, *X-ray diffraction procedures for polycrystalline and amorphous materials, John Wiley and Sons Inc, Canada* (1954).

54 Singh D & Mahajan A, *J Alloys Compd*, 644 (2015) 172.

55 Kumar N, Kishan H, Rao A & Awana V P S, *J Alloys Compd,* 502 (2010) 283.

56 Chang Y L, Huang Q & Ong C K, *J Appl Phys*, 91 (2002) 789.